The SCF^{FBXO46} ubiquitin ligase complex mediates degradation of the tumor suppressor FBXO31 and thereby prevents premature cellular senescence

Received for publication, August 14, 2018 Published, Papers in Press, August 31, 2018, DOI 10.1074/jbc.RA118.005354

Srinadh Choppara[‡§1], Sankaran Ganga[‡], Rajeshkumar Manne[‡§], Parul Dutta[‡§2], Shailza Singh[‡], and Manas Kumar Santra[‡3]

From the [‡]National Centre for Cell Science, NCCS Complex and the [§]Department of Biotechnology, Savitribai Phule Pune University, Ganeshkhind Road, Pune, Maharashtra 411007, India

Edited by Xiao-Fan Wang

The tumor suppressor F-box protein 31 (FBXO31) is indispensable for maintaining genomic stability. Its levels drastically increase following DNA damage, leading to cyclin D1 and MDM2 degradation and G_1 and G_2/M arrest. Prolonged arrest in these phases leads to cellular senescence. Accordingly, FBXO31 needs to be kept at low basal levels in unstressed conditions for normal cell cycle progression during growth and development. However, the molecular mechanism maintaining these basal FBXO31 levels has remained unclear. Here, we identified the F-box family SCF-E3 ubiquitin ligase FBXO46 (SCF^{FBXO46}) as an important proteasomal regulator of FBXO31 and found that FBXO46 helps maintain basal FBXO31 levels under unstressed conditions and thereby prevents premature senescence. Using molecular docking and mutational studies, we showed that FBXO46 recognizes an *RXXR* motif located at the FBXO31 C terminus to direct its polyubiquitination and thereby proteasomal degradation. Furthermore, FBXO46 depletion enhanced the basal levels of FBXO31, resulting in senescence induction. In response to genotoxic stress, ATM (ataxia telangiectasia-mutated) Ser/Thr kinase-mediated phosphorylation of FBXO31 at Ser-278 maintained FBXO31 levels. In contrast, activated ATM phosphorylated FBXO46 at Ser-21/Ser-67, leading to its degradation via FBXO31. Thus, ATM-catalyzed phosphorylation after DNA damage governs FBXO31 levels and FBXO46 degradation via a negative feedback loop. Collectively, our findings reveal that FBXO46 is a crucial proteasomal regulator of FBXO31 and thereby prevents senescence in normal growth conditions. They further indicate that FBXO46-mediated regulation of FBXO31 is abrogated following genotoxic stress to promote increased FBXO31 levels for maintenance of genomic stability.

Our genome is challenged by a multitude of DNA-damaging signals, such as UV radiations, chemical agents, and metabolic stress (1). It is essential to safeguard the genome from these stresses to prevent aging and cancer. For this purpose, there are crucial players acting at several steps to sense, transduce, and modify the DNA damage signal, to subsequently execute the appropriate rescue pathway. These players, from sensors to the executors, act in a concerted manner to elicit an effective DNA damage response (2). This response includes many biological events such as the activation of check points leading to arrest in the G_1 or G_2/M phase of the cell cycle and activation of the machinery that repairs the damaged genome (3, 4). However, the cells with irreparable DNA damage undergo either senescence or apoptosis through the activation of tumor suppressors (5–7).

F-box proteins play a crucial role in DNA damage response and repair. Typically, they function as the substrate receptor component of RING finger SCF[4] (SKP1-Cullin 1-F-box protein) E3 ubiquitin ligases (8, 9). The SCF E3 ubiquitin ligase complex consists of the three invariable components RBX1, Cullin 1, SKP1 and a variable component F-box protein. F-box proteins are grouped into three classes (FBXW, FBXL, and FBXO) based on the substrate interaction motif located in the C-terminal domain. The FBXW family of F-box proteins has a WD repeat domain; the FBXL family has a leucine-rich repeat domain, and the FBXO family has no specific substrate interaction domain (8). F-box proteins catalyze the ubiquitylation of various cellular substrates having diverse cellular functions, including cell signaling, metabolism, DNA damage response, and many more (10–15). Typically, it has been shown that F-box proteins recognize phosphorylated substrates to mediate their canonical polyubiquitination (lysine 48–linked ubiquitin conjugation to form a polyubiquitin chain) to direct proteasomal degradation (10). Several studies have documented that F-box proteins also catalyze the noncanonical ubiquitylation of their substrates (11). In addition, these F-box proteins may also cross-talk and regulate each other. For instance, the anti-apo-

This work was supported by Department of Biotechnology Grant BT/PR6690/GBD/27/475/2012 (to M. K. S.) and in part by the National Centre for Cell Science, Department of Biotechnology, Ministry of Science and Technology, Government of India (to M. K. S.). The authors declare that they have no conflicts of interest with the contents of this article.
This article contains Figs. S1–S4 and Tables S1 and S2.

[1] Research fellow of the Senior Council of Scientific and Industrial Research.
[2] Senior University Grants Commission (UGC) research fellow.
[3] To whom correspondence should be addressed: National Centre for Cell Science, NCCS Complex, Ganeshkhind Rd., Pune, Maharashtra 411007, India. Tel.: 91-2025708150; Fax: 91-2025692259; E-mail: manas@nccs.res.in.

[4] The abbreviations used are: SCF, SKP1-Cullin 1-F-box; ATM, ataxia telangiectasia-mutated; shRNA, short hairpin RNA; NS, nonsilencing; JNK, c-Jun N-terminal kinase; MEK, mitogen-activated protein kinase/extracellular signal-regulated kinase kinase; mTOR, mechanistic target of rapamycin; PVDF, polyvinylidene difluoride; Ni-NTA, nickel-nitrilotriacetic acid; Gy, gray; Ub, ubiquitin; TRCP, transducin repeat-containing protein.

ptotic protein FBXL18 promotes the degradation of the pro-apoptotic protein FBXL7 (16). It is also reported that β-transducin repeats-containing protein is involved in the degradation of FBXW2, although another report shows that SKP2 mediates the proteasomal degradation of β-TRCP (17). Interestingly, FBXW2 can also promote the degradation of SKP2, suggesting a complex interplay among the trio (18).

F-box protein FBXO31, a component of the SCF complex, acts as a dedicated DNA damage checkpoint protein to arrest the cells at G_1 and G_2/M phases of the cell cycle through two independent pathways (4, 19, 20). Following genotoxic stress, FBXO31 directly interacts with and mediates the degradation of MDM2 in p53-positive cells (19). A decrease in MDM2 results in increased levels of p53, which leads to growth arrest and senescence through transcriptional activation of *p21* (19). In p53-deficient cells, FBXO31 interacts with and mediates the degradation of cyclin D1 resulting in G_1 arrest upon genotoxic stress (4). Recently, FBXO31 has also been shown to target several other key cellular proteins associated with diverse biological functions, including the neuronal polarity protein Par6c, DNA replication licensing factor CDT1, the mitotic phase-specific transcription factor FOXM1, and the p38 MAPK signal activator MKK6 (21–24).

Despite having several cell cycle regulatory functions, cellular levels of FBXO31 in unstressed conditions remain low, as compared with the levels upon DNA damage (4, 20). Previous studies have shown that FBXO31 protein levels fluctuate during the cell cycle in unstressed cells (4, 20). However, how the levels of expression are maintained in unstressed conditions and the physiological relevance of its regulation are not fully elucidated. To address this question, we performed a RING finger (SCF and APC/C) E3 ligase screen to identify potential regulators of FBXO31. Among the several candidates that emerged out of the screen, we focused our investigations on FBXO46, the F-box family SCF-E3 ubiquitin ligase whose cellular function was unknown. In this study, we demonstrate two mechanisms: (*a*) how FBXO46 limits the senescence induction property of FBXO31 in unstressed cells, and (*b*) how FBXO31, in turn, regulates FBXO46 in a negative feedback loop and acts as a dedicated check point protein upon genotoxic stress. This coordinated regulation of the axis between FBXO31 and FBXO46 is essential for maintaining the genomic integrity and cellular homeostasis.

Results

Ectopic expression of FBXO46 leads to degradation of FBXO31

A previous study has shown that levels of FBXO31 protein oscillate during cell cycle progression (20). We observed that *FBXO31* mRNA levels remains unchanged during the cell cycle, indicating the existence of post-transcriptional or post-translational mechanisms that regulate FBXO31 protein levels throughout the cell cycle (data not shown). To delineate the factors that regulate FBXO31, we performed a RING finger E3 (SCF, APC/C) ligase screen and identified FBXO46 as one of the potential candidates that can regulate FBXO31.

To validate FBXO46 as a potential negative regulator of FBXO31, we ectopically expressed FBXO46 in increasing doses in HEK-293T cells. The results showed that FBXO46 significantly decreased FBXO31 levels in a dose-dependent manner (Fig. 1*A*). However, *FBXO31* mRNA levels remained unchanged, with significant ablation of post-transcriptional levels, following FBXO46 overexpression (Fig. 1, *B* and *C*), indicating the existence of post-transcriptional regulation. Consistent with these results, the addition of MG132 (a 26S proteasome inhibitor) inhibited FBXO46-mediated degradation of FBXO31 (Fig. 1*D*). To further confirm the proteasomal degradation of FBXO31 by FBXO46, the cycloheximide pulse–chase assay was performed. As shown in Fig. 1*E*, the half-life of FBXO31 significantly decreased in cells co-expressing FBXO46, as compared with empty vector transfected cells. For example, the half-life of FBXO31 decreased from 2.6 to 1.2 h (2.1-fold) upon overexpression of FBXO46 (Fig. 1*F*). Additionally, compared with WT FBXO46, the F-box motif-deleted mutant of FBXO46 (Myc-ΔF-FBXO46) failed to reduce FBXO31 levels, suggesting that FBXO46 degrades FBXO31 through the SCF complex (Fig. 1*G*). We next monitored the cellular localization of FBXO31 in cytoplasmic and nuclear extracts from cells expressing either vector or FBXO46. Immunoblot analysis showed the presence of FBXO31 predominantly in the cytoplasmic fraction, but we found that ectopically expressed FBXO46 degraded FBXO31 in both the cytoplasmic and nuclear fractions (Fig. 1*H*). Collectively, these observations suggest that SCF^{FBXO46} directs the proteasomal degradation of FBXO31 through the 26S proteasome.

Depletion of FBXO46 increases the stability of FBXO31

To determine whether FBXO46 maintains cellular levels of FBXO31, we generated a stable knockdown of FBXO46 (FBXO46 KD) in MCF7 cells using lentiviral shRNAs. Immunoblot analysis showed that FBXO31 levels significantly increased in the FBXO46 KD cells generated using three unrelated independent shRNAs targeting FBXO46 (Fig. 2*A*). Consistent with the results shown in Fig. 1*H*, the depletion of FBXO46 increased FBXO31 levels in both nuclear and cytoplasmic fractions, demonstrating that FBXO46 regulates the levels of FBXO31 in both locations (Fig. 2*B*). To further validate these results, cycloheximide pulse–chase experiments were performed in cells expressing nonsilencing (NS) and FBXO46 shRNA. The results showed that the stability of FBXO31 increased 1.8-fold in the FBXO46 knockdown cells as compared with the NS control (Fig. 2, *C* and *D*). Overall, these results suggest that FBXO46 regulates cellular levels of FBXO31.

FBXO46 maintains physiological levels of FBXO31 predominantly at the G_1/S phase of the cell cycle

As the results above indicate that FBXO46 regulates FBXO31 levels, we therefore examined whether FBXO46 targets FBXO31 at any specific phase of the cell cycle. To address this, both the WT (NS) and FBXO46 KD cells were synchronized using hydroxyurea at the G_1/S boundary. Following release from hydroxyurea at different time points, cells were analyzed for FBXO31 expression. As shown in Fig. 2, *E* and *F*, the expression levels of FBXO31 were significantly elevated throughout the cell cycle in FBXO46-depleted cells, being optimum at the G_1/S

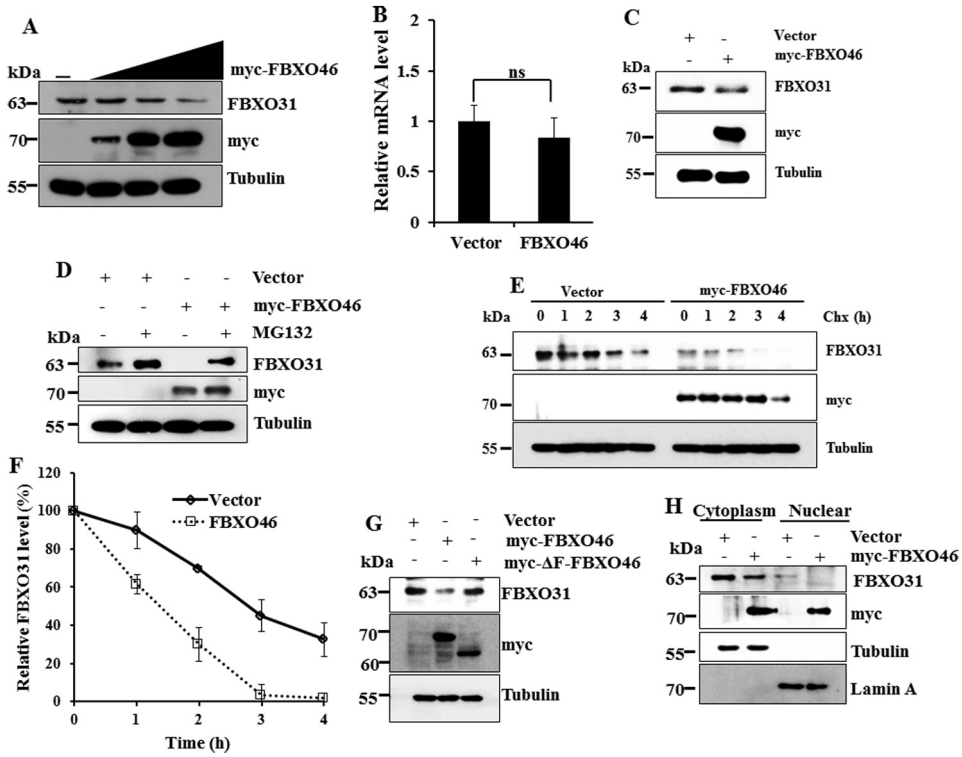

Figure 1. Ectopically expressed FBXO46 degrades FBXO31. *A*, HEK-293T cells were transfected with the indicated plasmids for 48 h, and the whole-cell lysates were immunoblotted with the indicated antibodies. Tubulin was used as the loading control. *B*, HEK-293T cells were transfected with the empty vector or Myc-FBXO46 for 48 h. Then, total RNA was isolated and subjected to cDNA preparation, and real time PCR was performed using SYBR Green as described under "Materials and methods." The experiment was repeated three times, and the data are presented as the mean ± standard deviation (S.D.). *ns*, statistically not significant. *C*, HEK-293T cells were transfected with either the vector control or Myc-FBXO46 for 48 h, and the whole-cell protein extracts were immunoblotted with the indicated antibodies. *D*, HEK-293T cells were transfected with the empty vector or Myc-FBXO46 for 36 h, and then cells were treated with and without 5 μM MG132 for 8 h. Whole-cell protein extracts were immunoblotted with the indicated antibodies. *E*, HEK-293T cells were transfected with the empty vector or Myc-FBXO46 for 36 h and then challenged with cycloheximide (*Chx*) (40 μg/ml) for the indicated time periods. Cells were then harvested, prepared whole-cell lysates, and immunoblotted with the indicated antibodies. *F*, levels of FBXO31 (in cycloheximide assay (*E*)) were quantified and normalized with the loading control. Expression levels of FBXO31 were then normalized to 100% at time 0. Data are presented as mean ± S.D. of three independent experiments. The protein levels of FBXO31 were normalized with the loading control tubulin and then set to 100% at time 0. The experiment was repeated three times and presented as the mean ± S.D. *G*, HEK-293T cells were transfected with the empty vector or Myc-FBXO46 or F-box motif deletion mutant of FBXO46 (Myc-ΔF-FBXO46) for 48 h. Cells were then harvested and lysed, and whole-cell protein extracts were immunoblotted with the indicated antibodies. *H*, HEK-293T cells were transfected with the empty vector or Myc-FBXO46 for 48 h, harvested, fractionated, and immunoblotted with the indicated antibodies. Tubulin and lamin A were used as the loading control for cytoplasmic and nuclear fractions, respectively. All the experiments were repeated three times unless otherwise stated.

phase. Similar results were also observed in nocodazole-synchronized cells (Fig. 2, *G* and *H*).

We next investigated whether stabilization of FBXO31 in the FBXO46 KD cells would lead to alteration in any cell cycle checkpoint. To address this, the cells expressing shRNA either for control (NS) or FBXO46 or FBXO31 along with FBXO46 were trapped at the G_2/M phase using nocodazole. As expected, the NS cells were arrested at the G_2/M phase, whereas a substantial population of the FBXO46 KD cells still remained at the G_1 phase (Fig. 2*I*). Interestingly, a maximum number of cells were trapped in the G_2/M phase following co-depletion of FBXO31 and FBXO46 (Fig. 2*I*). These observations collectively suggest that increased basal levels of FBXO31 in FBXO46 KD cells might be responsible for an increase in the G_1 population.

It has been reported previously that G_1 arrest is a prerequisite for senescence, and FBXO31 is known to facilitate G_1 arrest and senescence (4, 25). We therefore proceeded to check whether the FBXO46 KD cells have an increased propensity to undergo senescence. It was observed that the FBXO46 KD cells showed increased β-galactosidase activity, characteristic of senescent cells (Fig. 2, *J* and *K*).

FBXO46 interacts and promotes polyubiquitination of FBXO31

F-box proteins have the ability to interact with and promote polyubiquitination of their substrates through the SCF complex (14, 15, 21). Along these lines, we investigated the interaction between FBXO46 and FBXO31 by co-immunoprecipitation assay. Myc-FBXO46 was co-transfected either with an empty vector or FLAG–FBXO31 in HEK-293T cells. Immunoblot analysis revealed the presence of FBXO46 in the FBXO31 immunoprecipitates (Fig. 3*A*). In a reciprocal co-immunoprecipitation assay, FBXO31 was found to be present in the FBXO46 immunoprecipitates, suggesting that FBXO46 and FBXO31 interact with each other (Fig. 3*A*). These results were validated by endogenous co-immunoprecipitation of FBXO31 and FBXO46. As shown in Fig. 3*B*, an endogenous interaction between FBXO31 and FBXO46 was detected, which increased in the presence of MG132 (Fig. 3*B*). These observations suggested that FBXO46 physically interacts with FBXO31.

Canonical polyubiquitination by ubiquitin ligases is a prerequisite for any cellular protein to be degraded via the 26S proteasome (26, 27). We therefore examined whether proteasomal

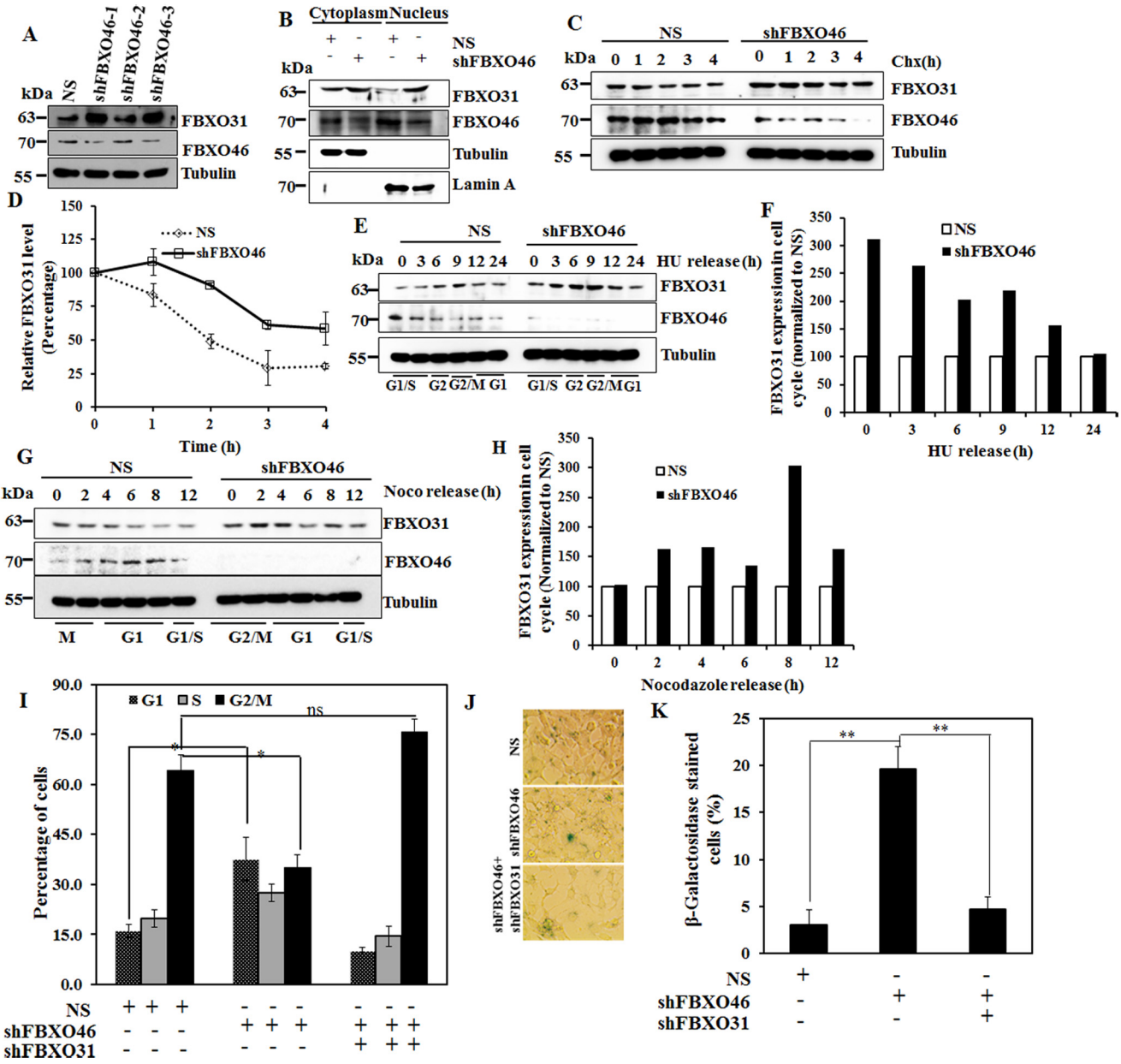

Figure 2. Depletion of FBXO46 leads to stabilization of FBXO31. *A*, MCF7 cells were transduced with lentivirus of scramble shRNA (NS) or different shRNA against FBXO46, and stable cell lines were generated as described under "Materials and methods." Whole-cell lysates of NS and FBXO46 knockdown cells were immunoblotted with the indicated antibodies. These data are representative of three independent experiments. *B*, NS and FBXO46 knockdown cells were fractionated into cytoplasmic and nuclear fractions as described under "Materials and methods" and immunoblotted for the indicated proteins. These data are representative of three independent experiments. *C*, NS and FBXO46 knockdown cells were pulsed with cycloheximide for the indicated periods, and the protein extracts were immunoblotted with the indicated antibodies. These data are representative of three independent experiments. *Chx,* cycloheximide. *D*, densitometric analysis of FBXO31 immunoblot in *C*. The levels of FBXO31 were quantified and normalized with the loading control tubulin. The expression levels of FBXO31 were then normalized to 100% at time 0. Data are presented as mean ± S.D. of three independent experiments. *E*, NS and FBXO46 knockdown cells were synchronized with 0.25 mM hydroxyurea for 22 h. Then, synchronized cells were released and collected at the indicated time points. Whole-cell protein extracts were immunoblotted with the indicated antibodies. These data are representative of two independent experiments. *F*, levels of FBXO31 were quantified from blots in *E* and normalized with the loading control tubulin. Expression levels of FBXO31 were then normalized to 100% in the NS cells at each time point. The data are presented as the mean of two independent experiments. *G*, NS and FBXO46 knockdown cells were synchronized by growing in 125 nM nocodazole (*Noco*) containing media for 16 h. Then mitotic cells were released and collected at the indicated time points. Whole-cell protein extracts were immunoblotted with the indicated antibodies. These data are representative of two independent experiments. *H*, levels of FBXO31 were quantified from the blots in *G* and normalized with the loading control tubulin. Expression levels of FBXO31 were then normalized to 100% at each time point for the NS cells. The levels of FBXO31 in FBXO46 knockdown cells were then calculated with respect to NS cells. The data are presented as the mean of two independent experiments. *I*, NS or shFBXO46 or shFBXO46 and shFBXO31 stably expressing cells were treated with 125 nM nocodazole for 16 h, and cells were collected, and the collected cells were subjected to FACS analysis. The experiment was repeated three times, and the data are presented as the mean ± S.D. *ns* ($p > 0.05$), * ($p < 0.05$). *J*, NS or shFBXO46 or shFBXO46 and shFBXO31 stably expressing MCF7 cells were stained for β-gal activity. These data are representative of three independent experiments. *K*, quantification of senescent cells of NS, FBXO46, FBXO46–FBXO31 knockdown cells. The data are presented as the mean ± S.D. of three independent experiments. **, $p < 0.01$.

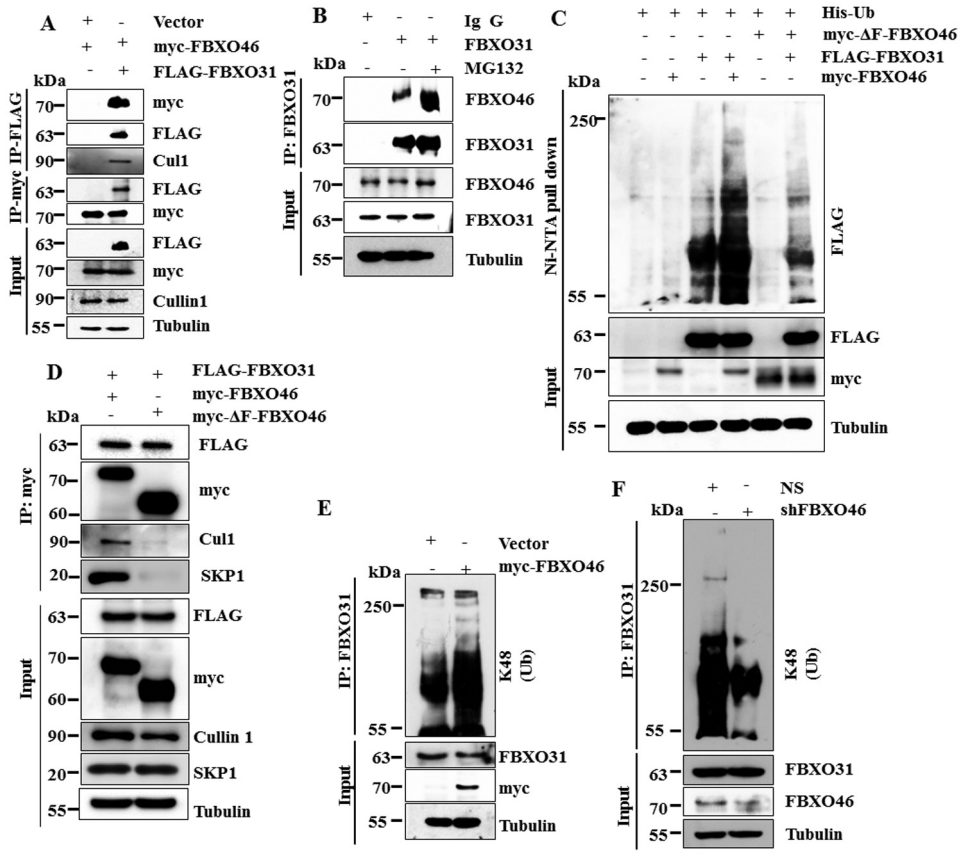

Figure 3. FBXO46 interacts with FBXO31 and promotes its polyubiquitination. *A*, HEK-293T cells were transfected with Myc-FBXO46 in combination with either vector control or FLAG–FBXO31 for 36 h, and transfected cells were then treated with 5 μM MG132 for 8 h. Whole-cell extracts were prepared and immunoprecipitated (*IP*) with the indicated antibodies, and immunoprecipitates were immunoblotted with the indicated antibodies. These data are representative of three independent experiments. *B*, HEK-293T cells were grown in the absence or presence of 5 μM MG132 for 8 h. Whole-cell protein extracts were immunoprecipitated either with the anti-IgG or FBXO31 antibody. Immunoprecipitates were resolved by SDS-PAGE and immunoblotted with the indicated antibodies. These data are representative of three independent experiments. *C*, HEK-293T cells were transfected with His–Ub along with either vector control or FLAG–FBXO31 or Myc-FBXO46 or Myc-ΔF-FBXO46 or in combination with FLAG–FBXO31 and Myc-FBXO46 or in combination with FLAG–FBXO31 and Myc-ΔF-FBXO46 for 36 h. The transfected cells were then treated with 5 μM MG132 for 8 h. Whole-cell proteins extracts were used to pull down His–Ub using Ni-NTA beads and immunoblotted with the indicated antibodies. These data are representative of three independent experiments. *D*, HEK-293T cells were co-transfected with FLAG–FBXO31 and Myc-FBXO46 or FLAG–FBXO31 and Myc-ΔF-FBXO46 for 36 h. The transfected cells were then grown in the presence of 5 μM MG132 for 8 h. Whole-cell protein extracts were immunoprecipitated with anti-Myc antibody. Immunoprecipitated and input protein lysates were immunoblotted with the indicated antibodies. These data are representative of two independent experiments. *E*, HEK-293T cells were transfected either with the vector control or Myc-FBXO46 for 36 h. Transfected cells were then incubated with 5 μM MG132 for 8 h, and whole-cell protein extracts were immunoprecipitated with the anti-FBXO31 antibody. Immunoprecipitates and input protein extracts were immunoblotted with the indicated antibodies. These data are representative of two independent experiments. *F*, whole-cell protein extracts of NS and FBXO46 knockdown cells were immunoprecipitated with the anti-FBXO31 antibody. Immunoprecipitates and input proteins were immunoblotted with the indicated antibodies. These data are representative of two independent experiments.

degradation of FBXO31 occurred through polyubiquitination. To address this, we performed an *in vivo* ubiquitination assay in which His-ubiquitin, FLAG–FBXO31, Myc-FBXO46, and Myc-ΔF-FBXO46 were co-expressed followed by Ni-NTA pull-down to capture the ubiquitylated proteins. As shown in Fig. 3*C*, only co-expression of Myc-FBXO46 promoted robust polyubiquitination of FBXO31, whereas Myc-ΔF-FBXO46 failed to polyubiquitinate FBXO31. To examine why ΔF-FBXO46 fails to polyubiquitinate FBXO31, we checked the interaction of Myc-ΔF-FBXO46 with FLAG–FBXO31. The results revealed that Myc-ΔF-FBXO46 efficiently interacts with FBXO31 but fails to form the SCF complex (Fig. 3*D*).

Next, we examined the involvement of the lysine residue of ubiquitin in polyubiquitination and found that FBXO46 promoted the Lys-48 –linked polyubiquitination of FBXO31 (Fig. 3*E*). These observations were further supported by reduction in Lys-48 –linked ubiquitination of FBXO31 in FBXO46 KD cells (Fig. 3*F*). Thus, results taken together suggest that FBXO46 interacts with FBXO31, promotes Lys-48 –linked polyubiquitination, and thereby facilitates proteasomal degradation through the 26S proteasome.

FBXO46 recognizes the RXXR motif positioned at the C terminus of FBXO31

The interaction between FBXO46 and FBXO31 prompted us to map the FBXO46-binding motif within the FBXO31 protein. To address this, we generated a series of N-terminal deletion mutants of FBXO31 (Fig. 4*A*) and studied their interaction with FBXO46 following co-expression by co-immunoprecipitation. The results revealed that FBXO46 degrades all the deletion mutants of FBXO31 suggesting that FBXO46 recognizes the C-terminal domain of FBXO31 (Fig. 4*B*). To further delineate the specific region of FBXO31 recognized by FBXO46, we searched for the motif present in the C-terminal deletion

mutant (ΔD8-FBXO31) of FBXO31 using *in silico* modeling. Analysis revealed the presence of an R*XX*R motif at the C terminus of FBXO31 (Fig. 4*C*).

The structural model of FBXO31 was obtained from the Robetta server (28). After validation, the model analysis indicated that FBXO31 was accurate and had the least errors. The peptides of FBXO31 listed in Table S1 were docked in the FBXO46 model. Following docking, the pose analysis indicated that four R*XX*R motifs had the best binding score. Among these peptides, the best affinity was shown by the motif YPRTCRM located in the C terminus (ΔD8-FBXO31), with binding energy −6.5 kcal mol^{-1} (Fig. 4, *D* and *E*). Detailed structural analysis indicated that all these peptide motifs interacted in the same binding pocket even in the blind docking mode. The peptide bound at the cavity was more charged and possessed hydrophobic residues. The detailed docking results are given in the docking scores (Table S1). Atomic level interaction analysis using Ligplot^{+} (29) indicated that all these motifs of FBXO31 have hydrogen bond interaction with charged residues like Glu-216, Arg-217, Thr-440, and Asp-442 of FBXO46. This suggested that biochemically these motifs are highly charged, and these peptide motifs showed specific interactions with FBXO31. The specificity of these peptide motifs can be visualized in the given figures in which the FBXO46 structural model is represented in

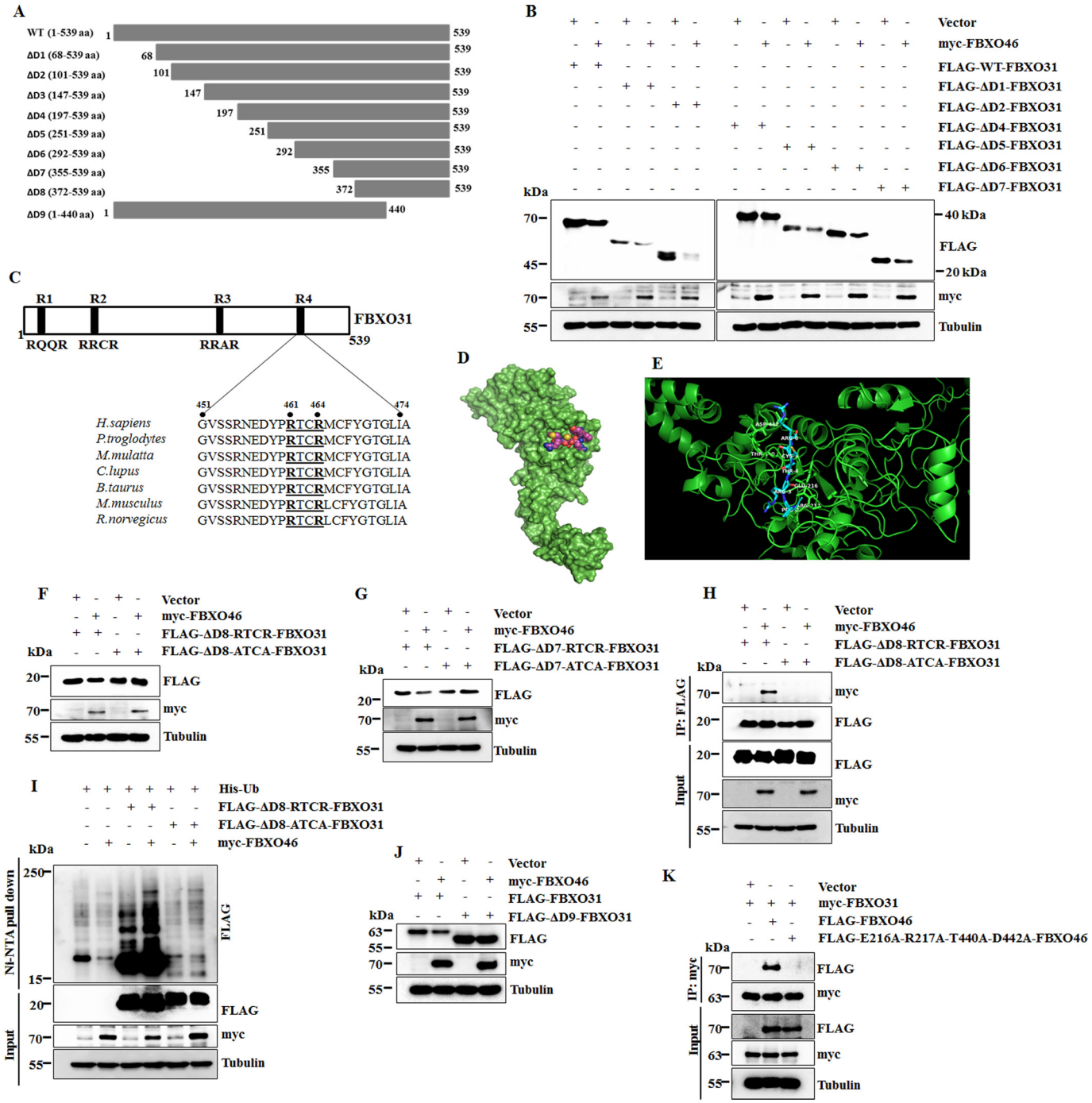

green cartoon and *green surface,* and peptides are shown in the *sphere* representation (Fig. 4*D*). All the atomic level interactions are represented through Ligplots; peptide residues are represented in ball and stick models, and hydrogen bonds are shown as green dashed lines in Fig. S1*A*. All van der Waal interacting residues are represented as *red dashed crescents* (Fig. S1*A*).

The above *in silico* analysis predicted that the R*XX*R motif located in ΔD8-FBXO31 has the highest binding affinity for FBXO46. Further analysis of all the R*XX*R motifs present in FBXO31 revealed that the motif located in ΔD8-FBXO31 is highly conserved among the mammals (Fig. 4*C* and Fig. S1*B*). Thus, to experimentally validate the importance of the R*XX*R motif located in ΔD8-FBXO31 in its degradation by FBXO46, we mutated YPRTCRM to YPATCAM. Next, we checked the level of WT and mutant ΔD8-FBXO31 in the presence of FBXO46. Interestingly, FBXO46 failed to degrade the ΔD8-FBXO31 mutant but did degrade the WT ΔD8-FBXO31 (Fig. 4*F*). To further confirm the importance of the C-terminal R*XX*R motif of FBXO31 in FBXO46-mediated degradation, we checked the sequence of different deletion mutants of FBXO31 and found that ΔD7-FBXO31 has a D-box motif (R*XX*L) and also a C-terminal R*XX*R motif. Interestingly, both ΔD7-FBXO31 and ΔD8-FBXO31 share the same R*XX*R motif. Co-expression of FBXO46 either with WT ΔD7-FBXO31 or R*XX*R mutant (ATCA) ΔD7-FBXO31 resulted in degradation of only the WT ΔD7-FBXO31 and not the mutant, suggesting that FBXO46 specifically targets the R*XX*R motif and not the D-box motif of ΔD7-FBXO31 (Fig. 4*G*).

To understand whether the failure of FBXO46 to degrade ΔD8-ATCA-FBXO31 resulted from a disruption in their interactions, a co-immunoprecipitation assay was performed. We observed that FBXO46 specifically interacted only with the WT ΔD8-FBXO31 but not with the mutant ΔD8-FBXO31, further indicating that FBXO46 recognizes the R*XX*R motif located in the C terminus of FBXO31 (Fig. 4*H*). Additionally, we also compared polyubiquitination of ΔD8-FBXO31 and the mutant ΔD8-FBXO31 and found that only the ΔD8-FBXO31 was significantly polyubiquitylated in the presence of FBXO46 (Fig. 4*I*).

Knowing that FBXO31 harbors four R*XX*R motifs and the C-terminal R*XX*R motif is adequate to promote proteasomal degradation of ΔD8-FBXO31 by FBXO46, we proceeded to elucidate the roles of the other three N-terminal R*XX*R motifs (Fig. 4*C*). We checked the stability of a C-terminal deletion mutant ΔD9-FBXO31 harboring the other three R*XX*R motifs, in the absence and presence of FBXO46. Immunoblot results revealed that FBXO46 was unable to degrade ΔD9-FBXO31, indicating that FBXO46 specifically recognizes the R*XX*R motif located at the C terminus of FBXO31 (Fig. 4*J* and Fig. S1*C*).

To further confirm the importance of the C-terminal ^{461}R*XX*R^{464} motif, we examined the stability of the WT and ^{461}A*XX*A^{464} mutant of full-length FBXO31 in NS and FBXO46 KD cells and found that the WT FBXO31 is significantly stabilized in the FBXO46 KD cells (Fig. S1*D*). In contrast, the expression levels of the C-terminal R*XX*R mutant FBXO31 remain similar in both the NS and FBXO46 KD cells (Fig. S1*D*). Likewise, FBXO46 fails to promote polyubiquitination of the C-terminal ^{461}A*XX*A^{464} motif mutant of full-length FBXO31 due to abrogation of the interaction (Fig. S1, *E* and *F*). Taken together, these results suggest that FBXO46 interacts with FBXO31 by recognizing the C-terminal R*XX*R motif and promotes its proteasomal degradation.

Furthermore, we proceeded to identify the region of FBXO46 that is involved in the interaction with FBXO31. *In silico* analysis using the Robetta server predicted Glu-216, Arg-217, Thr-440, and Asp-442 of FBXO46 to be interacting with the C-terminal YPRTCRM motif of FBXO31 (Fig. 4, *D* and *E,* and Fig. S1*A*). To experimentally validate the involvement of these residues, we mutated them to alanine. Co-immunoprecipitation results revealed that interaction between FBXO31 and FBXO46 remained intact with FBXO46E216A but declined with FBXO46R217A/T440A/D442A (Fig. S1*G*) indicating that Glu-216 of FBXO46 might not be involved in the interaction with FBXO31. However, mutation of all four residues resulted in abrogation of the interaction between FBXO31 and FBXO46 (Fig. 4*K*) indicating that, Arg-217, Thr-440, and Asp-442 residues of FBXO46 are essential for the interaction with FBXO31.

JNK, MEK, and mTOR-mediated phosphorylation is essential for the FBXO46-mediated degradation of FBXO31

Typically, F-box proteins recognize the phosphorylated forms of substrates for interaction and subsequent proteasomal degradation (30). We therefore asked whether the FBXO46–

Figure 4. FBXO46 degrades FBXO31 by recognizing the R*XX*R motif located at the C terminus. *A*, schematic diagram representing the generation of different deletion mutants of FBXO31. *B*, different deletion mutants of FLAG–FBXO31 were co-expressed in the absence and presence of Myc-FBXO46 for 48 h, and then the protein extracts were immunoblotted with the indicated antibodies. These data are representative of two independent experiments. *C*, schematic representation of the conservation of the ^{461}R*XX*R^{464} motif among mammals. *D*, surface view representation of FBXO46 (*green surface* and *green spheres*) docked with the FBXO31 peptide (*pink spheres*). *E*, representation of FBXO31 peptide "YPRTCRM" docked to FBXO46 (*green*). *F*, HEK-293T cells were transfected with FLAG–ΔD8–FBXO31 and mutant FLAG-ΔD8-FBXO31 in the absence and presence of Myc-FBXO46 for 48 h. Whole-cell protein extracts were immunoblotted with the indicated antibodies. These data are representative of three independent experiments. *G*, HEK-293T cells were transfected with the FLAG–ΔD7–FBXO31 and mutant FLAG–ΔD7–FBXO31 in the absence and presence of Myc-FBXO46 for 48 h. Whole-cell protein extracts were immunoblotted with the indicated antibodies. These data are representative of three independent experiments. *H*, HEK-293T cells were transfected with either FLAG–ΔD8–FBXO31 or mutant FLAG–ΔD8–FBXO31 in the absence and presence of Myc-FBXO46 for 36 h. The transfected cells were then treated with 5 μM MG132 for 8 h. Whole-cell protein extracts were immunoprecipitated (*IP*) with anti-FLAG antibody, and immunoprecipitates were immunoblotted with the indicated antibodies. These data are representative of two independent experiments. *I*, HEK-293T cells were transfected with His–Ub either with FLAG–ΔD8–FBXO31 or mutant FLAG–ΔD8–FBXO31 in the absence and presence of Myc-FBXO46 for 36 h. The transfected cells were then treated with 5 μM MG132 for 8 h. Whole-cell protein extracts were subjected to pulldown assay with Ni-NTA beads, and eluates were immunoblotted with anti-FLAG antibody. These data are representative of two independent experiments. *J*, HEK-293T cells were co-transfected with FLAG–FBXO31 or FLAG–ΔD9–FBXO31 either with vector control or Myc-FBXO46 for 48 h. Whole-cell protein extracts were immunoblotted with the indicated antibodies. These data are representative of three independent experiments. *K*, HEK-293T cells were co-transfected either with FLAG–FBXO46 or FLAG–E216A/R217A/T440A/D442A–FBXO46 along with Myc-FBXO31 for 36 h. The transfected cells were then treated with 5 μM MG132 for 8 h. Whole-cell protein extracts were immunoprecipitated with anti-Myc antibody, and the immunoprecipitates and input protein extracts were probed for the indicated proteins. These data are representative of two independent experiments.

FBXO31 interaction was sufficient to degrade FBXO31, or whether the phosphorylated form of FBXO31 was required for its recognition and degradation. To address this, we checked whether any kinase could phosphorylate FBXO31. *In silico* analysis predicted that JNK, MEK, and mTOR may phosphorylate FBXO31 at Thr-419 and Ser-480 and therefore may play a role in the stability of ΔD8-FBXO31 (Fig. 5*A*). We then sought to investigate whether these kinases phosphorylate ΔD8-FBXO31. Immunoblotting results demonstrated that inhibition of JNK (Fig. 5*B*) and MEK (Fig. 5*C*) led to significant suppression in phosphorylation of serine and threonine, although inhibition of mTOR (Fig. 5*D*) led to a noticeable decline only in threonine phosphorylation (Fig. 5, *B–D*). Following this, we determined the relevance of these phosphorylations in FBXO46-mediated degradation of ΔD8-FBXO31. Interestingly, FBXO46 failed to degrade ΔD8-FBXO31 upon inhibition of either JNK or MEK or mTOR suggesting that the phosphorylation of ΔD8-FBXO31 by these kinases is decisive for its degradation by FBXO46 (Fig. 5, *E–G*).

Next we determined whether the *in silico* predicted phosphorylation sites Thr-419 and Ser-480 of ΔD8-FBXO31 and full-length FBXO31 are important for FBXO46-mediated degradation of ΔD8-FBXO31. Immunoblot results demonstrated that FBXO46 fails to degrade the full-length FBXO31(T419A), FBXO31(S480A), mutant ΔD8-FBXO31(T419A), and mutant ΔD8-FBXO31(S480A), signifying the importance of these phosphorylation sites (Fig. S2, *A* and *B*, and Fig. 5, *H* and *I*). Furthermore, we performed polyubiquitination experiments, and the results showed that FBXO46 fails to polyubiquitylate ΔD8-FBXO31(T419A) and ΔD8-FBXO31(S480A), confirming that phosphorylation at these residues is required for FBXO46-mediated degradation of ΔD8-FBXO31 (Fig. 5*J* and Fig. S2*C*). Similar results were also found for the full-length FBXO31(T419A) and FBXO31(S480A) mutants (Fig. S2*D*). However, FBXO46 interacts with FBXO31 independent of the phosphorylation status of FBXO31, suggesting that these phosphorylations are essential for polyubiquitination of FBXO31 by FBXO46 but are dispensable for interactions between them (Fig. 5*K* and Fig. S2*E*). Finally, we checked the phosphorylation status of the FBXO31 mutant following JNK inhibition. The results revealed that phosphoserine/phosphothreonine levels of ΔD8-FBXO31 sharply declined (Fig. S2, *F* and *G*). In contrast, phosphoserine levels of ΔD8-S480A-FBXO31 and phosphothreonine levels of ΔD8-T419A-FBXO31 remained unaltered following inactivation of JNK, indicating that these sites might be the putative phosphorylation of JNK (Fig. S2, *F* and *G*).

FBXO46 cannot degrade FBXO31 upon genotoxic stresses

Previous studies from our group and other groups have shown that FBXO31 acts as a dedicated DNA damage checkpoint protein (4, 19, 24, 31, 32). It directs activation of p53 and arrests the cells at the G_1 phase of the cell cycle through proteasomal degradation of cyclin D1 following genotoxic stresses (4, 19). We therefore sought to determine whether the stabilization of FBXO31 following DNA damage is due to an interference in the FBXO31–FBXO46 axis. To test this, we monitored the levels of FBXO31 and FBXO46 in cells treated with different DNA-damaging agents. As expected, FBXO31 was stabilized following various genotoxic stresses (Fig. 6*A*). Interestingly, the levels of FBXO46 significantly decreased upon exposure to various DNA-damaging agents (Fig. 6*A*). We further investigated whether ectopic expression of FBXO46 could suppress the stabilization of FBXO31 following genotoxic stress. As shown in Fig. 6*B*, following exposure of MCF7 cells to ionizing radiation, the ectopically expressed FBXO46 also failed to prevent stabilization of FBXO31. Similar results were also obtained following treatment of the MCF7 cells with UV radiation (Fig. 6*C*) indicating that FBXO46 may not facilitate the ablation of FBXO31 under genotoxic stresses.

A previous study reported that FBXO31 is stabilized through ATM-mediated phosphorylation at Ser-278 following DNA damages (4). We therefore investigated whether phosphorylation at Ser-278 results in FBXO31 being resistant to degradation by FBXO46. Immunoblotting results revealed that FBXO46 was unable to degrade the phosphomimetic mutant of FBXO31 even in the absence of DNA damage (Fig. S3*A*) indicating that Ser-278 phosphorylation in FBXO31 is important to prevents its degradation by FBXO46.

Next, we checked the populations of NS, FBXO46 KD, and FBXO31–FBXO46 KD cells at different cell cycle phases 24 h post-irradiation and found a substantial fraction of the FBXO46 KD cells to be present at the G_1 phase of the cell cycle (Fig. 6*D*). The increased population of FBXO46 knockdown cells at the G_1 phase following DNA damage might be, at least in part, due to the elevated levels of FBXO31 (Fig. S3*B*). Then, we determined the extent of senescence induction in these cells following DNA damage. It was observed that depletion of FBXO46 significantly increased the population of senescent cells, which was inhibited upon co-depletion with FBXO31 (Fig. 6, *E* and *F*).

The serine/threonine kinase, ATM, is rapidly and specifically activated in response to DNA double-strand damage and phosphorylates substrates having the SQ/TQ sites (33). Analysis of the FBXO46 amino acid sequence revealed the presence of two putative ATM phosphorylation sites located at Ser-21 and Ser-67, which are conserved in mammals (Fig. 6*G*). We therefore performed a series of experiments to evaluate whether ATM has any role in the ablation of FBXO46 upon genotoxic stress. First, cells were exposed to ionizing radiation in the absence and presence of an ATM inhibitor. The results showed that the DNA damage-induced reduction of FBXO46 is significantly blocked upon inactivation of ATM (Fig. 6*H*). To determine whether Ser-21 and Ser-67 have a role in the ablation of FBXO46 during genotoxic stress, we performed site-directed mutagenesis to generate S21A-FBXO46 and S67A-FBXO46 mutants in which serine was mutated to alanine. As shown in Fig. 6, *I* and *J*, both these mutants failed to undergo ablation following genotoxic stress, indicating that phosphorylation of Ser-21 and Ser-67 by ATM might be essential for reduction of its expression. However, phosphorylation of FBXO46 at these sites is dispensable for the interaction with the FBXO31 (Fig. S3*C*).

FBXO31 degrades FBXO46 under genotoxic stresses

We next performed a series of experiments to examine how the expression levels of FBXO46 decline following genotoxic stresses. First, we performed real time RT-PCR in cells sub-

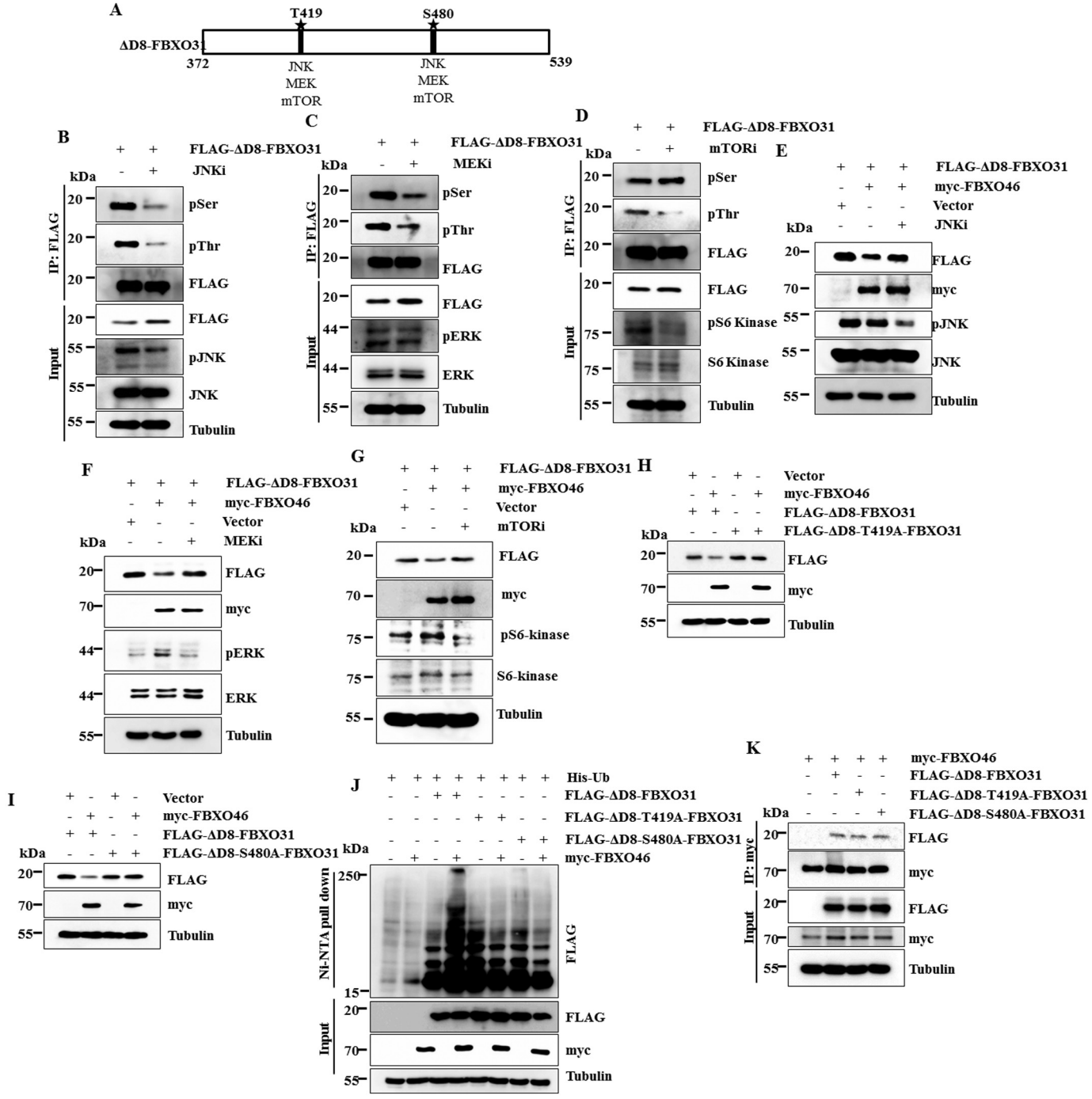

Figure 5. JNK, MEK, and mTOR-mediated phosphorylation of FBXO31 facilitate its degradation by FBXO46. *A*, *in silico* predicted JNK, MEK, and mTOR phosphorylation sites in FLAG–ΔD8–FBXO31. *B–D*, HEK-293T cells were transfected with FLAG–ΔD8–FBXO31 for 36 h, and then the transfected cells were incubated in the absence and presence of either JNK (*B*) or MEK (*C*) or mTOR (*D*) inhibitor for 24 h. Cell lysates were immunoprecipitated (*IP*) with anti-FLAG antibody followed by immunoblotting with the indicated antibodies. These data are representative of three independent experiments. *E–G*, HEK-293T cells were co-transfected with FLAG–ΔD8–FBXO31 either with vector control or Myc-FBXO46 for 36 h. The transfected cells were treated with either JNK (*E*) or MEK (*F*) or mTOR (*G*) inhibitor for 24 h. Cell lysates were immunoblotted with the indicated antibodies. These data are representative of three independent experiments. *H*, HEK-293T cells were co-transfected with FLAG–ΔD8–FBXO31/FLAG–ΔD8–T419A–FBXO31 along with either vector control or Myc-FBXO46 for 48 h. Cell lysates were then immunoblotted with the indicated antibodies. These data are representative of two independent experiments. *I*, HEK-293T cells were co-transfected with FLAG–ΔD8–FBXO31/FLAG–ΔD8–T480A–FBXO31 either with vector control or Myc-FBXO46 for 48 h. Cell lysates were then immunoblotted with the indicated antibodies. These data are representative of two independent experiments. *J*, HEK-293T cells were co-transfected with the indicated plasmids for 36 h. The transfected cells were then treated with 5 μM MG132 for 8 h. The whole-cell lysates were used to pull down ubiquitin by Ni-NTA beads, and the eluates were immunoblotted with the indicated antibodies. These data are representative of four independent experiments. *K*, HEK-293T cells were co-transfected with Myc-FBXO46 and either one of FLAG–ΔD8–FBXO31, FLAG–ΔD8–T419A–FBXO31, and FLAG–ΔD8–S480A–FBXO31 for 36 h. The transfected cells were treated with MG132 for 8 h, and following that, the cells were lysed, and the whole-cell lysates were immunoprecipitated with anti-Myc antibody. The immunoprecipitates and input protein extracts were immunoblotted with the indicated antibodies. These data are representative of two independent experiments.

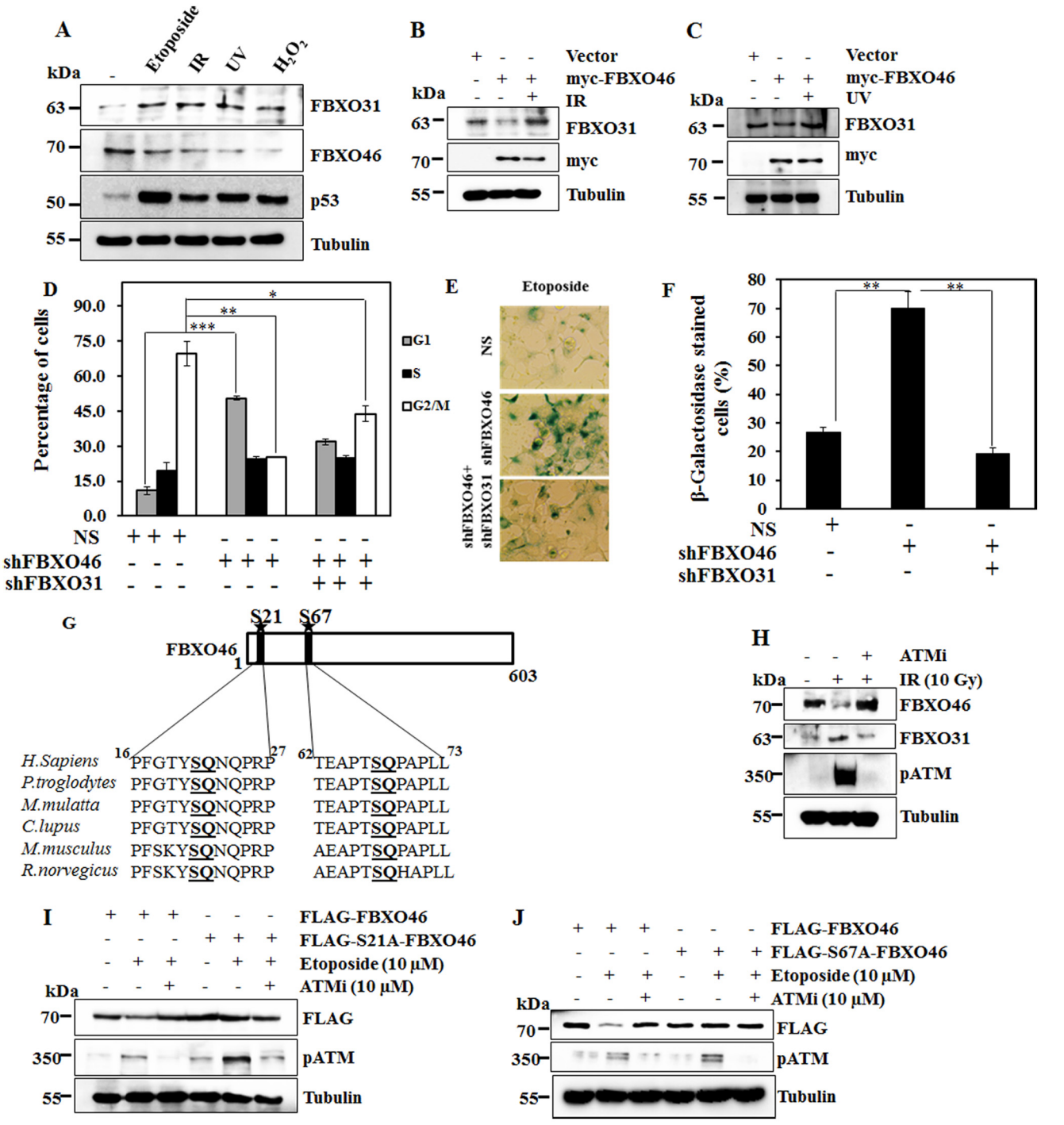

Figure 6. FBXO46 does not interfere with the stabilization of FBXO31 under genotoxic stresses. *A,* MCF7 cells were either untreated or treated with 10 μM etoposide for 24 h or 10 Gy ionizing radiation for 4 h or 100 mJ/m^2 UV for 4 h or 0.05% H_2O_2 for 2 h. The cells were then lysed and immunoblotted with the indicated antibodies. These data are representative of three independent experiments. *B* and *C*, MCF7 cells were transfected either with the vector control or Myc-FBXO46 for 36 h. The transfected cells were then treated with 10 Gy ionizing radiation (*B*) for 4 h or 100 mJ/m^2 UV for 4 h (*C*). MCF7 cell lysates were immunoblotted with the indicated antibodies. These data are representative of two independent experiments. *D,* NS or shFBXO46 or shFBXO46 and shFBXO31 stably expressing MCF7 cells were treated with 10 Gy γ-irradiation (*IR*), and cells were collected at 24 h post-irradiation, and FACS analysis was performed. Data are presented as mean ± S.D. of three independent experiments. These data are representative of three independent experiments. * ($p < 0.05$), ** ($p < 0.01$), and *** ($p < 0.001$) as indicated. *E* and *F*, NS or shFBXO46 or shFBXO46 and shFBXO31 stably expressing MCF7 cells were treated with etoposide (500 nM) for 6 days, and the cells were then stained for β-gal activity (*E*). β-Gal–positive cells were counted and plotted as percentage (*F*). Data are presented as mean ± S.D. of three independent experiments. These data are representative of three independent experiments. ** ($p < 0.01$) as indicated. *G*, schematic of ATM phosphorylation sites in FBXO46. *H*, MCF7 cells were pre-treated with 10 μM ATM inhibitor for 8 h as indicated. Cells were then either untreated or treated with ionizing radiation (10 Gy) for 4 h. The cell lysates were immunoblotted with the indicated antibodies. These data are representative of two independent experiments. *I,* MCF7 cells were transfected with FLAG–FBXO46 or FLAG–S21A–FBXO46 for 36 h. The transfected cells were treated with 10 μM etoposide for 24 h in the absence and presence of 10 μM ATM inhibitor in the last 12 h. The cell lysates were immunoblotted with the indicated antibodies. These data are representative of three independent experiments. *J*, MCF7 cells were transfected with FLAG–FBXO46 or FLAG–S67A–FBXO46 for 36 h, and the transfected cells were treated with 10 μM etoposide for 24 h in the absence and presence of 10 μM ATM inhibitor in the last 12 h. Cell lysates were immunoblotted with the indicated antibodies. These data are representative of three independent experiments.

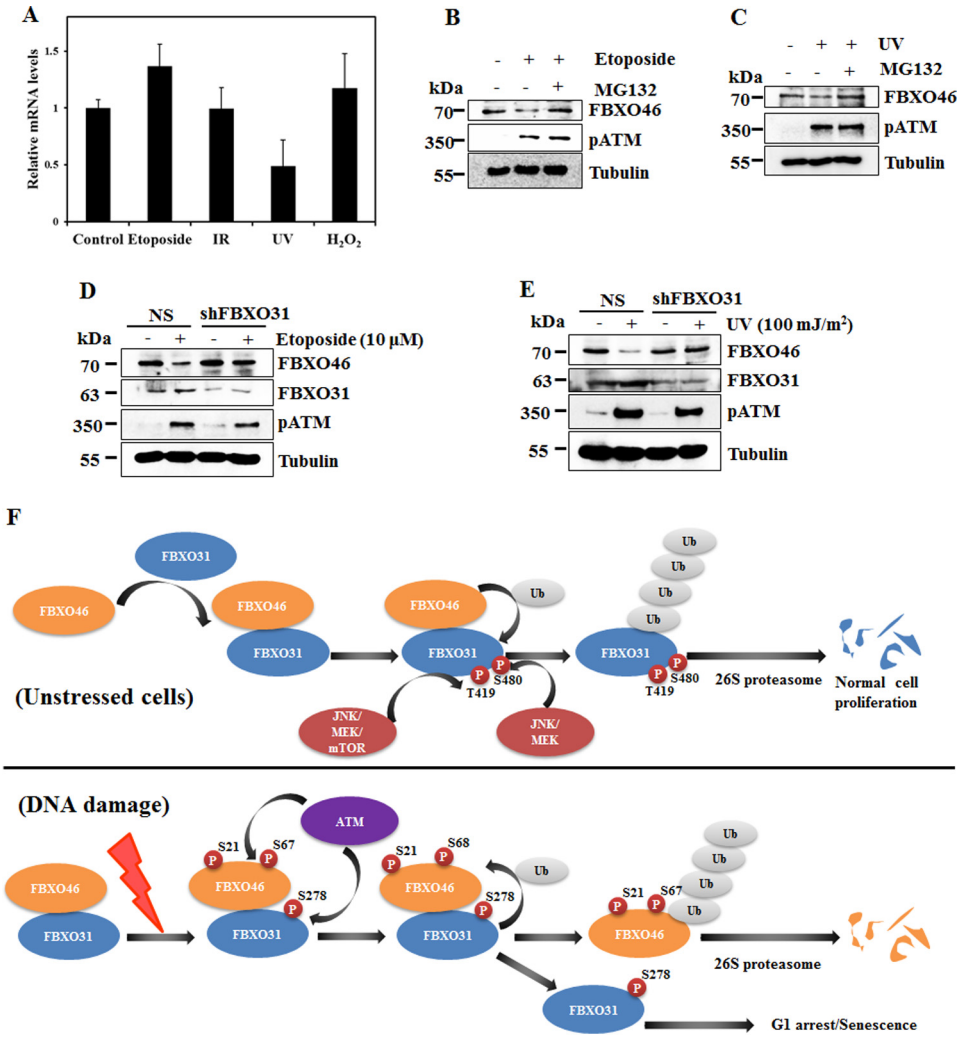

Figure 7. FBXO31 degrades FBXO46 under genotoxic stresses through 26S proteasome. *A*, MCF7 cells were treated with the indicated genotoxic stress-inducing agents as described in Fig. 6*A*. Total RNA was isolated, reverse-transcribed, and real-time PCR was performed using SYBR Green. These data are represented as a mean ± S.D. from three independent experiments. *B*, cells were either untreated or treated with 10 μM etoposide for 24 h in the absence and presence of 5 μM MG132 in the last 8 h. Whole-protein extracts were immunoblotted with the indicated antibodies. These data are representative of two independent experiments. *C*, MCF cells were either left untreated or treated with UV (100 mJ/m^2) in the presence and absence of MG132. Whole-protein extracts were immunoblotted with the indicated antibodies. These data are representative of two independent experiments. *D*, NS and FBXO31KD cells were either untreated or treated with 10 μM etoposide and probed for the indicated proteins. These data are representative of three independent experiments. *E*, NS and FBXO31KD cells were either untreated or treated with UV (100 mJ/m^2), and the whole-cell lysates were separated on SDS-PAGE and probed for the indicated proteins. These data are representative of three independent experiments. *F*, model representing the summary of work.

jected to various DNA-damaging agents. The results showed no significant changes in the mRNA levels of *FBXO46*, except with UV radiation (Fig. 7*A*), where the levels were moderately decreased (Fig. 7*A*). FBXO46 levels were then examined following genotoxic stress in the absence and presence of MG132. Immunoblot analysis revealed that treatment with this proteasome inhibitor inhibited etoposide or UV-induced degradation of FBXO46 (Fig. 7, *B* and *C*). In addition, we performed the cycloheximide chase assay, whose results revealed that the turnover of FBXO46 accelerated following exposure to either etoposide or UV radiation (Fig. S4, *A* and *B*). These results suggested that the expression of FBXO46 is largely suppressed at the post-transcriptional level following DNA damage. However, UV radiation-induced DNA damage suppressed the expression of FBXO46 both at the transcriptional and post-translational levels.

Previously, we have reported that FBXO31 is stabilized through ATM-mediated phosphorylation at Ser-278 following DNA damages (4). Our current results show that following DNA damage, the levels of FBXO31 and FBXO46 are inversely correlated (Fig. 6*A*). We therefore asked whether FBXO31 is involved in the regulation of FBXO46 following genotoxic stresses. To address this question, we generated stable FBXO31 KD cells and subjected them to DNA damage. As expected, FBXO46 was degraded following DNA damages in the cells expressing nonsilencing shRNA, whereas FBXO46 levels were unaltered in FBXO31KD cells (Fig. 7, *D* and *E*). However, the F-box motif of FBXO31 is not important for the interaction between FBXO31 and FBXO46 (Fig. S4*C*). These results suggested that FBXO31 targets FBXO46 for proteasomal degradation following genotoxic stress. Collectively, our study supports the existence of a feedback loop that allows FBXO31 to target

FBXO46 upon genotoxic stress, thus allowing the accumulation of FBXO31, which leads to the activation of further downstream signaling required for combating the stress.

Discussion

The tumor suppressor FBXO31 is present at low levels in unstressed cells, and its levels oscillate during the cell cycle, where it is involved in regulating the G_1 and G_2 phases (4, 19). In this study, as outlined in the model above, we report for the first time that the F-box protein, FBXO46, maintains the cellular levels of the tumor suppressor FBXO31 through proteasomal degradation in the unstressed cells, which prevents premature senescence and genomic instability (Fig. 7*F*). Following genotoxic stress, ATM-mediated phosphorylation of FBXO31 at Ser-278 and FBXO46 at Ser-21/Ser-67 leads to the stabilization of FBXO31 and down-regulation of FBXO46. We posit that phosphorylation at Ser-278 marks as a negative signal for proteasomal degradation of FBXO31, and phosphorylation at Ser-21 and Ser-67 directs the proteasomal degradation of FBXO46 by FBXO31. We have identified here the existence and mechanism of a feedback loop where stabilized FBXO31 targets FBXO46 for proteasome-mediated degradation, following DNA damage. This is additional evidence of an E3 ligase F-box protein cross-talking with another F-box protein in a context-dependent manner to ensure genomic stability. Consistent with our current observations, previous studies have also documented such cross-talks among the F-box proteins in different contexts, such as between SKP2 and FBXW2 (18), FBXL18 and FBXL7 (19), and β-TRCP and FBXW2 (18).

Because overexpression of FBXO31 or its stabilization following genotoxic stresses can induce senescence or growth arrest (4, 19, 20), the continuation of an unperturbed cell cycle requires FBXO31 to be maintained at low levels in the unstressed cells. This raises the question whether the varying FBXO31 levels in the normal cycling cells and post-DNA damage are due to post-transcriptional or post-translational regulation. Recent studies have reported the role of miRNA (miR-17, miR-20a, miR-93, miR-106a, and miR-210) in the post-transcriptional regulation of FBXO31 (34–36). Our earlier study also showed that mir-93 and mir-106a suppress the translation of FBXO31 in the unstressed condition, which is reversed following genotoxic stress (36). Based on these reports, we infer that miRNAs can regulate FBXO31 in a context-dependent manner, but cannot account for the varying FBXO31 levels at different phases of the cell cycle. Despite the fact that it is critical to maintain optimal cellular levels of FBXO31, no study has yet deciphered the physiological regulation of FBXO31. Our results convincingly demonstrate that FBXO31 is a cellular target of FBXO46.

The cellular function of the SCF E3 ubiquitin ligase substrate receptor FBXO46 was not known previously. This is the first study that documents the functional role of FBXO46 in the cellular context, where we also identify FBXO31 as its *bona fide* substrate. As revealed by our findings, FBXO46 promotes polyubiquitination of FBXO31 and maintains its physiological protein levels through the proteasome-mediated pathway.

Our *in silico* biochemical and mutational analysis revealed that the YPRTCRM motif at the FBXO31 C terminus serves as the recognition site for FBXO46 (Fig. 4). We have also demonstrated for the first time that the R*XX*R motif in FBXO31 serves as a signature sequence, which is recognized by FBXO46, to degrade FBXO31. Interestingly, a few previous reports have also suggested that the R*XX*R motif could have possible cellular roles like heparin binding for a T-cell response following adeno-associated virus infection or that the R*XX*R motif could be recognized as a proteolytic cleavage site (37, 38). Many other E3 ubiquitin ligases recognize similar recognition motifs in their substrates for degradation, for example, DSG*XX*(S/T) serves as a recognition signal for βTRCP-mediated regulation (9).

It is known from the literature that F-box proteins interact with phosphorylated substrates to direct their proteasomal degradation (30). Here, we also find that FBXO31 stability depends on three well-known kinases, JNK, MEK, and mTOR, in the unstressed cells, which phosphorylate FBXO31, and this phosphorylation triggers polyubiquitination (Fig. 5). Although MEK and JNK phosphorylate FBXO31 at Thr-419 and Ser-480, MEK, JNK, and mTOR share the common phosphorylation site (Thr-419). Thus, the phosphorylated form of FBXO31 is indispensable for its degradation by FBXO46 but not for the interaction. Consistent with these results, previous studies have reported the role of JNK or MEK or ERK kinases in the phosphorylation of cIAP, Bim, and Bid and their role in promoting degradation (39–43).

Tumor suppressor FBXO31 has several important cellular roles such as promoting G_1 and G_2/M arrest following DNA damage, thereby allowing cells to repair the damaged DNA and also preventing the proliferation of genomically unstable cells (4, 19). Apart from this, FBXO31 might also play other roles in the DNA damage repair and maintenance of genomic integrity through activation of the DNA repair pathway, and in the inhibition of apoptosis induction (21, 25, 44). Considering its multiple roles in the cell, FBXO31 levels would need to be tightly regulated in the unstressed cells and maintained at high levels during stress. We have recently shown that whereas basal levels of FBXO31 are maintained by miR-93 and miR-106a at the translational level, and by APC/C at the proteasomal level, they fail to regulate the expression levels of FBXO31 under genotoxic stresses (36, 45). In turn, FBXO31 inhibits the expression of these miRNAs upon genotoxic stresses (36). Along the same lines, in this study we have deciphered another function of FBXO31, which is degradation of FBXO46 via a negative feedback loop, following genotoxic stress. We have also identified here that ATM-mediated phosphorylation of FBXO31 and FBXO46 plays a critical role, leading to stabilization of one and destabilization of the other. Our results clearly demonstrated that following genotoxic stresses, the phosphorylation at Ser-278 stabilizes FBXO31, and Ser-21/Ser-67–phosphorylated FBXO46 is then targeted by FBXO31 for proteasome-mediated degradation. This regulation is important in maintaining the genomic stability. This study thus opens a path toward understanding the other cellular components that are targeted by FBXO46 in the cell cycle and during genotoxic stress.

Materials and methods

Cell culture, RNAi-mediated knockdowns, and treatments

HEK-293T and MCF7 cells were obtained from Prof. Michael R. Green (University of Massachusetts Medical School, Worcester, MA) and were maintained in Dulbecco's modified Eagle's medium (Gibco) supplemented with 10% fetal bovine serum (Gibco), 100 mg/ml penicillin, and 100 milliunits/ml streptomycin in 5% CO_2 at 37 °C.

Lentivirus was generated in HEK-293T cells following transfection of pPax2, pMD2.G, and lentiviral shRNA using polyethyleneimine. After 48 h of incubation, the virus-containing media were collected and filtered through a 0.45-μm syringe filter. For generating stable knockdown cell lines, cells were stably transduced in the presence of Polybrene (10 μg/ml) with the following lentivirus shRNAs from Open Biosystems (shFBXO46-1-V2LHS_47109, shFBXO46-2-V2LHS_47104, shFBXO46-3-V3LHS_385151, and shFBXO31-V2HS_157523). The transduced cells were then selected with puromycin (1 μg/ml) for 10 days. Chemical inhibitors for JNK (420119), MEK (662005), mTOR (553210), and proteasome inhibitor MG132 (474790) were purchased from Calbiochem. ATM inhibitor was obtained from TOCRIS (3544). Cells were treated with MG132 (5 μM) for 8 h, JNK (5 μM) for 24 h, MEK (125 nM) for 24 h, mTOR (50 nM) for 24 h, or ATM (10 μM) for 12 h. For cell synchronization studies, cells were treated with hydroxyurea (Sigma, H8627) for 22 h. Cycloheximide (C1988) and etoposide (E1383) were obtained from Sigma. H_2O_2 was procured from ThermoFisher Scientific (18755).

For UV irradiation, the growth media were removed, and the cells were washed two times with PBS and then exposed to UV radiation (100 mJ/m^2) using a Hoefer Scientific UV crosslinker. For ionizing radiation treatment, cells were irradiated with 10 Gy for 4 h using a Co^{60} irradiator.

Plasmids and generation of site-directed mutants

His-ubiquitin was procured from Addgene. The Myc-FBXO31 plasmid was a kind gift from Prof. David F Callen (University of Adelaide and Hanson Institute, Australia). We re-cloned FBXO31 in the p3×FLAG-Myc-CMV-26 vector (Sigma) by using the restriction sites of EcoRI and HindIII. Serial N-terminal deletion mutants of FBXO31 were generated in the 3×FLAG-26 vector using the EcoRI and HindIII sites. FBXO46 plasmid was obtained from Origene. FBXO46 was re-cloned in the p3×FLAG–CMV-14 vector at the EcoRI site using an infusion cloning kit from Takara. F-box motif-deleted FBXO46 (ΔF-FBXO46) was generated in the p3×FLAG–CMV-14 vector. Site-directed mutagenesis techniques were used to generate all the point mutants. Sequences of the primers used are listed in Table S2.

Immunoblot and co-immunoprecipitation

Protein extracts were prepared, and immunoblotting and co-immunoprecipitation were performed as described previously (4) using the following antibodies: Cell Signaling Technologies, cullin 1 (4995); Lys-48 (Ub) (8081); pan-pSer (9606); pan-pThr (9391); pERK (9106); S6 kinase (9202); pS6 kinase (9205); and pATM (13050). Antibodies against the following were obtained as follows: FBXO31 (Sigma, F4431); α-tubulin (Sigma, T5168); FLAG (Sigma, F1804); Myc (Roche Applied Science, 11667149001); and FBXO46 antibody (Abcam, ab129454) were obtained. The antibodies against the following proteins were obtained from Santa Cruz Biotechnology: lamin A (sc-71481); pJNK (sc-6254); JNK (sc-7345); ERK (sc-94); and p53 (sc-126). Briefly, cells were washed twice with ice-cold PBS, harvested, and collected by centrifugation. Cell extracts were prepared by lysing the cells in lysis buffer containing 50 mM Tris, pH 7.4, 200 mM NaCl, 50 mM NaF, 1 mM Na_3VO_4, 0.5% Triton X-100, and a protease inhibitor mixture on ice for 20 min as described previously (4). Protein concentration was determined by using the Bradford assay (46). Samples were prepared in Laemmli buffer, and proteins were separated using SDS-PAGE with Tris-glycine-SDS running buffer and transferred onto the PVDF membrane using Tris-glycine transfer buffer containing 20% methanol. Nonspecific sites on the membranes were then blocked with 5% skimmed milk or 5% BSA in TBST buffer followed by overnight incubation in the respective primary antibody at 4 °C with gentle rocking. The next day, the membranes were washed five times with TBST buffer and incubated with the appropriate horseradish peroxidase-conjugated secondary antibody for 1 h at room temperature. Finally, the blots were washed five times with TBST buffer and developed using chemiluminescence reagents (Pierce).

For co-immunoprecipitation, cells were pretreated with 5 μM MG132 for 8 h. The protein extracts (800 μg) in IP lysis buffer (50 mM Tris, pH 7.4, 200 mM NaCl, 50 mM NaF, 1 mM Na_3VO_4, 0.1% Triton X-100) were incubated with 2 μg of the primary antibody overnight at 4 °C with gentle rotation. The next day, the washed recombinant protein G–agarose beads were added to the antigen–antibody complex and incubated for 2 h at 4 °C with gentle rotation. The beads were then washed three times with the IP lysis buffer, and the bound proteins (immunoprecipitates) were eluted in Laemmli buffer followed by boiling for 5 min. Total cell extracts and immunoprecipitates were loaded onto SDS-PAGE and transferred to the PVDF membrane followed by immunoblotting with the indicated antibodies.

Ubiquitination assay

For the *in vivo* ubiquitination assay, cells were co-transfected with plasmids expressing His-tagged ubiquitin, Myc-FBXO46, Myc-ΔF-FBXO46 and FLAG–FBXO31. Cells were pre-treated with MG132, 8 h prior to the extract preparation. The ubiquitylated proteins were purified under denaturing conditions using Ni-NTA beads and immunoblotted using an anti-FLAG antibody.

For the Lys-48 (Ub)–linked polyubiquitination assay shown in Fig. 3, *D* and *E*, protein extracts from cells expressing either the vector or Myc-FBXO46 or scrambled shRNA or shRNA against FBXO46 were immunoprecipitated with anti-FBXO31 antibody and immunoblotted using the Lys-48 –Ub antibody (Cell Signaling Technology, 8081S).

Real time RT-PCR

Cells were collected in the TRIzol reagent (Invitrogen), and total RNA was isolated according to the manufacturer's proto-

col. Total RNA (1 μg) was reverse-transcribed using the cDNA synthesis kit (Takara), followed by real time PCR using SYBR Green (Takara). The relative levels were normalized to the internal control glyceraldehyde-3-phosphate dehydrogenase. Sequences of the primers used are listed in Table S2.

Cycloheximide pulse–chase assay

Cells were pulsed with cycloheximide (40 μg/ml) and chased at the indicated time periods. Cells were then collected, and the prepared protein extracts were immunoblotted with the indicated antibodies using the procedure as described above. Protein expression at each time point was measured by densitometry analysis using the ImageJ software and normalized with tubulin. The expression at zero time was taken as 100%.

Cell cycle analysis

For cell cycle analysis, cells were synchronized with hydroxyurea (0.25 mM for 22 h). Cells were then released from synchronization by washing twice with incomplete media followed by growing in complete media for the indicated time periods. Half of the cells were used for FACS analysis, and the rest were collected for immunoblot analysis as described above.

Cytoplasmic and nuclear extracts preparation

Cells were harvested and washed twice with ice-cold PBS. Cells were pelleted at 3000 rpm for 2 min at 4 °C. The pelleted cells were resuspended in the hypotonic buffer A (10 mM HEPES-K^+, pH 7.5, 10 mM KCl, 1.5 mM $MgCl_2$, 0.1 mM DTT, 0.5% Triton X-100, and protease inhibitor mixture), incubated on ice for 5 min, and then spun down at 2500 × *g* for 5 min at 4 °C. The supernatant containing the cytoplasmic fraction was transferred to a fresh microcentrifuge tube without disturbing the pellet. The pellet was resuspended in the wash buffer (10 mM HEPES, pH 7.5, 10 mM KCl, 1.5 mM $MgCl_2$, and 0.1 mM DTT), incubated for 2 min on ice, and pelleted at 3000 × *g* for 2 min, and this step was repeated twice to remove the cytoplasmic contaminants completely. The final pellet was lysed with the cell lysis buffer (50 mM Tris, pH 7.4, 200 mM NaCl, 50 mM NaF, 1 mM Na_3VO_4, 0.5% Triton X-100, and protease inhibitor mixture) on ice for 20 min and then centrifuged at 10,000 × *g* for 15 min at 4 °C. The supernatants were collected as the nuclear fraction. Both the cytoplasmic and nuclear fractions were immunoblotted to examine the indicated protein as described above.

β-Gal staining

MCF7 cells stably expressing either the NS or shFBXO46 or shFBXO46 and shFBXO31 were treated with 500 nM etoposide on alternate days for a period of 6 days, and then the cells were allowed to grow for another 5 days. The senescence induction was observed as flattened morphology. The extent of induction of senescence was determined by staining for the β-gal enzyme activity at pH 6.0, as described previously (47). Images were captured using an EVOS microscope, and the percent of β-gal–positive senescent cells was calculated.

Molecular modeling of FBXO31, FBXO46, and peptide motifs

To predict the three-dimensional structures of FBXO31 and FBXO46, the mentioned sequences were submitted to the Robetta server (28). The Robetta server uses an automated structure prediction pipeline where initial domain prediction is done using the Ginzhu module, and later, the structures for predicted domains of the given sequences would be predicted using comparative modeling or *ab initio* methods. For FBXO46, the 3D structure of all the domains was predicted using comparative modeling, and for FBXO31, two of the five domains were predicted using *ab initio* methods. After the successful structure prediction of all the domains, they were threaded using the Modeler 9.16 (48) software. The best models among the predicted ones were chosen on the basis of DOPE score and GA 341. After modeling, all the models were verified and validated using SAVES (Structure Analysis and Verification server), which includes Procheck (49), What Check and ERRAT (50), Verify 3D (51), and PROVE (52) along with Prosa (53) web server. All the given peptide motifs' three-dimensional structures were predicted using the PEPstr (54).

Molecular docking of the given peptide motifs with FBXO46

The best models among the predicted structures were preprocessed with the AutoDock tools program of MGL tools 1.5.6 (55). Similarly, the predicted peptide structures were also preprocessed. Molecular Docking was then performed using the AutoDock Vina program (56). After successful completion of the docking process, the best peptide–protein complexes were identified based on the docking/binding scores. The best protein–peptide complexes at both the residue level and atomic level interactions were mapped using the Ligplot+ (29) tool. All the molecular graphics were generated using PyMOL (Delano Scientific).

Author contributions—S. C., S. S., and M. K. S. conceptualization; S. C., S. G., and S. S. data curation; S. C., R. M., P. D., S. S., and M. K. S. formal analysis; S. C. and M. K. S. validation; S. C., S. G., R. M., P. D., S. S., and M. K. S. investigation; S. C., S. G., R. M., P. D., S. S., and M. K. S. methodology; S. C., S. G., and S. S. writing-original draft; P. D. and M. K. S. writing-review and editing; M. K. S. supervision; M. K. S. funding acquisition; M. K. S. project administration.

Acknowledgments—We thank Prof. Michael R. Green and Prof. David F. Callen for providing reagents. We thank Dr. Sunil K. Malonia, Dr. Jayati Mullick, Dr. Ajay Pillai, and Dr. Jyoti Rao for editing the manuscript.

References

1. Ciccia, A., and Elledge, S. J. (2010) The DNA damage response: making it safe to play with knives. *Mol. Cell* **40,** 179–204 CrossRef Medline
2. Maréchal, A., and Zou, L. (2013) DNA damage sensing by the ATM and ATR kinases. *Cold Spring Harb. Perspect. Biol.* **5,** a012716 CrossRef Medline
3. Zhou, B.-B., and Elledge, S. J. (2000) The DNA damage response: putting checkpoints in perspective. *Nature* **408,** 433–439 CrossRef Medline
4. Santra, M. K., Wajapeyee, N., and Green, M. R. (2009) F-box protein FBXO31 mediates cyclin D1 degradation to induce G_1 arrest after DNA damage. *Nature* **459,** 722–725 CrossRef Medline
5. Khoo, K. H., Hoe, K. K., Verma, C. S., and Lane, D. P. (2014) Drugging the p53 pathway: understanding the route to clinical efficacy. *Nat. Rev. Drug Discov.* **13,** 217–236 CrossRef Medline
6. Sabin, R. J., and Anderson, R. M. (2011) Cellular senescence–its role in cancer and the response to ionizing radiation. *Genome Integr.* **2,** 7 CrossRef Medline

7. Elmore, S. (2007) Apoptosis: a review of programmed cell death. *Toxicol. Pathol.* **35,** 495–516 CrossRef Medline
8. Jin, J., Cardozo, T., Lovering, R. C., Elledge, S. J., Pagano, M., and Harper, J. W. (2004) Systematic analysis and nomenclature of mammalian F-box proteins. *Genes Dev.* **18,** 2573–2580 CrossRef Medline
9. Frescas, D., and Pagano, M. (2008) Deregulated proteolysis by the F-box proteins SKP2 and β-TrCP: tipping the scales of cancer. *Nat. Rev. Cancer* **8,** 438–449 CrossRef Medline
10. Newton, K., Matsumoto, M. L., Wertz, I. E., Kirkpatrick, D. S., Lill, J. R., Tan, J., Dugger, D., Gordon, N., Sidhu, S. S., Fellouse, F. A., Komuves, L, French, D. M., Ferrando, R. E., Lam, C., Compaan, D., *et al.* (2008) Ubiquitin chain editing revealed by polyubiquitin linkage-specific antibodies. *Cell* **134,** 668–678 CrossRef Medline
11. Chan, C. H., Li, C. F., Yang, W. L., Gao, Y., Lee, S. W., Feng, Z., Huang, H. Y., Tsai, K. K., Flores, L. G., Shao, Y., Hazle, J. D., Yu, D., Wei, W., Sarbassov, D., Hung, M. C., *et al.* (2012) The Skp2-SCF E3 ligase regulates akt ubiquitination, glycolysis, herceptin sensitivity, and tumorigenesis. *Cell* **149,** 1098–1111 CrossRef Medline
12. Zhou, Z., He, M., Shah, A. A., and Wan, Y. (2016) Insights into APC/C: from cellular function to diseases and therapeutics. *Cell Div.* **11,** 9 CrossRef Medline
13. Bassermann, F., and Pagano, M. (2010) Dissecting the role of ubiquitylation in the DNA damage response checkpoint in G_2. *Cell Death Differ.* **17,** 78–85 CrossRef Medline
14. Wang, G., Chan, C. H., Gao, Y., and Lin, H. K. (2012) Novel roles of Skp2 E3 ligase in cellular senescence, cancer progression, and metastasis. *Chin. J. Cancer* **31,** 169–177 CrossRef Medline
15. Nakayama, K. I., and Nakayama, K. (2006) Ubiquitin ligases: cell-cycle control and cancer. *Nat. Rev. Cancer* **6,** 369–381 CrossRef Medline
16. Liu, Y., Lear, T., Zhao, Y., Zhao, J., Zou, C., Chen, B. B., and Mallampalli, R. K. (2015) F-box protein Fbxl18 mediates polyubiquitylation and proteasomal degradation of the pro-apoptotic SCF subunit Fbxl7. *Cell Death Dis.* **6,** e1630 CrossRef Medline
17. Wei, S., Chu, P. C., Chuang, H. C., Hung, W. C., Kulp, S. K., and Chen, C. S. (2012) Targeting the oncogenic E3 ligase Skp2 in prostate and breast cancer cells with a novel energy restriction-mimetic agent. *PLoS ONE* **7,** e47298 CrossRef Medline
18. Xu, J., Zhou, W., Yang, F., Chen G., Li, H., Zhao, Y., Liu, P., Li, H., Tan, M., Xiong, X., and Sun, Y. (2017) The β-TrCP-FBXW2-SKP2 axis regulates lung cancer cell growth with FBXW2 acting as a tumour suppressor. *Nat. Commun.* **8,** 14002 CrossRef Medline
19. Malonia, S. K., Dutta, P., Santra, M. K., and Green, M. R. (2015) F-box protein FBXO31 directs degradation of MDM2 to facilitate p53-mediated growth arrest following genotoxic stress. *Proc. Natl. Acad. Sci. U.S.A.* **112,** 8632–8637 CrossRef Medline
20. Kumar, R., Neilsen, P. M., Crawford, J., McKirdy, R., Lee, J., Powell, J. A., Saif, Z., Martin, J. M., Lombaerts, M., Cornelisse, C. J., Cleton-Jason, A. M., Callen, D. F. (2005) FBXO31 is the chromosome 16q24.3 senescence gene, a candidate breast tumor suppressor, and a component of an SCF complex. *Cancer Res.* **65,** 11304–11313 CrossRef Medline
21. Vadhvani, M., Schwedhelm-Domeyer, N., Mukherjee, C., and Stegmüller, J. (2013) The centrosomal E3 ubiquitin ligase FBXO31-SCF regulates neuronal morphogenesis and migration. *PLoS ONE* **8,** e57530 CrossRef Medline
22. Johansson, P., Jeffery, J., Al-Ejeh, F., Schulz, R. B., Callen, D. F., Kumar, R., and Khanna, K. K. (2014) SCF-FBXO31 E3 ligase targets DNA replication factor Cdt1 for proteolysis in the G_2 phase of cell cycle to prevent re-replication. *J. Biol. Chem.* **289,** 18514–18525 CrossRef Medline
23. Jeffery, J. M., Kalimutho, M., Johansson, P., Cardenas, D. G., Kumar, R., and Khanna, K. K. (2017) FBXO31 protects against genomic instability by capping FOXM1 levels at the G_2/M transition. *Oncogene* **36,** 1012–1022 CrossRef Medline
24. Liu, J., Han, L., Li, B., Yang, J., Huen, M. S., Pan, X., Tsao, S. W., and Cheung, A. L. (2014) F-box only protein 31 (FBXO31) negatively regulates p38 mitogen-activated protein kinase (MAPK) signaling by mediating lysine 48-linked ubiquitination and degradation of mitogen-activated protein kinase kinase 6 (MKK6). *J. Biol. Chem.* **289,** 21508–21518 CrossRef Medline
25. Agami, R., and Bernards, R. (2000) Distinct initiation and maintenance mechanisms cooperate to induce G_1 cell cycle arrest in response to DNA damage. *Cell* **102,** 55–66 CrossRef Medline
26. Jentsch, S., and Schlenker, S. (1995) Selective protein degradation: a journey's end within the proteasome. *Cell* **82,** 881–884 CrossRef Medline
27. Hochstrasser, M. (1996) Ubiquitin-dependent protein degradation. *Annu. Rev. Genet.* **30,** 405–439 CrossRef Medline
28. Kim, D. E., Chivian, D., and Baker, D. (2004) Protein structure prediction and analysis using the Robetta server. *Nucleic Acids Res.* **32,** W526–W531 CrossRef Medline
29. Laskowski, R. A., and Swindells, M. B. (2011) LigPlot+: Multiple ligand-protein interaction diagrams for drug discovery. *J. Chem. Inf. Model.* **51,** 2778–2786 CrossRef Medline
30. Skowyra, D., Craig, K. L., Tyers, M., Elledge, S. J., and Harper, J. W. (1997) F-box proteins are receptors that recruit phosphorylated substrates to the SCF ubiquitin-ligase complex. *Cell* **91,** 209–219 CrossRef Medline
31. Shiloh, Y. (2009) FBXO31: a new player in the ever-expanding DNA damage response orchestra. *Sci. Signal.* **2,** pe73 Medline
32. Jia, L., and Sun, Y. (2009) F-box proteins FBXO31 and FBX4 in regulation of cyclin D1 degradation upon DNA damage. *Pigment Cell Melanoma Res.* **22,** 518–519 CrossRef Medline
33. Matsuoka, S., Ballif, B. A., Smogorzewska, A., McDonald, E. R., 3rd., Hurov, K. E., Luo, J., Bakalarski, C. E., Zhao, Z., Solimini, N., Lerenthal, Y., Shiloh, Y., Gygi, S. P., and Elledge, S. J. (2007) ATM and ATR substrate analysis reveals extensive protein networks responsive to DNA damage. *Science* **316,** 1160–1166 CrossRef Medline
34. Liu, D., Xia, H., Wang, F., Chen, C., and Long, J. (2016) MicroRNA-210 interacts with FBXO31 to regulate cancer proliferation cell cycle and migration in human breast cancer. *Onco Targets Ther.* **9,** 5245–5255 CrossRef Medline
35. Zhang, X., Kong, Y., Xu, X., Xing, H., Zhang, Y., Han, F., Li, W., Yang, Q., Zeng, J., Jia, J., and Liu, Z. (2014) F-box protein FBXO31 is down-regulated in gastric cancer and negatively regulated by miR-17 and miR-20a. *Oncotarget* **5,** 6178–6190 Medline
36. Manne, R. K., Agrawal, Y., Bargale, A., Patel, A., Paul, D., Gupta, N. A., Rapole, S., Seshadri, V., Subramanyam, D., Shetty, P., and Santra, M. K. (2017) A microRNA/ubiquitin ligase feedback loop regulates slug-mediated invasion in breast cancer. *Neoplasia* **19,** 483–495 CrossRef Medline
37. Vandenberghe, L. H., Wang, L., Somanathan, S., Zhi, Y., Figueredo, J., Calcedo, R., Sanmiguel, J., Desai, R. A., Chen, C. S., Johnston, J., Grant, R. L., Gao, G., and Wilson, J. M. (2006) Heparin binding directs activation of T cells against adeno-associated virus serotype 2 capsid. *Nat. Med.* **12,** 967–971 CrossRef Medline
38. de Zoeten, E. F., Lee, I., Wang, L., Chen, C., Ge, G., Wells, A. D., Hancock, W. W., and Ozkaynak, E. (2009) Foxp3 processing by proprotein convertases and control of regulatory T cell function. *J. Biol. Chem.* **284,** 5709–5716 CrossRef Medline
39. He, W., Wang, Q., Srinivasan, B., Xu, J., Padilla, M. T., Li, Z., Wang, X., Liu, Y., Gou, X., Shen, H. M., Xing, C., and Lin, Y. (2014) A JNK-mediated autophagy pathway that triggers c-IAP degradation and necroptosis for anticancer chemotherapy. *Oncogene* **33,** 3004–3013 CrossRef Medline
40. Brichese, L., Barboule, N., Heliez, C., and Valette, A. (2002) Bcl-2 phosphorylation and proteasome-dependent degradation induced by paclitaxel treatment: consequences on sensitivity of isolated mitochondria to bid. *Exp. Cell Res.* **278,** 101–111 CrossRef Medline
41. Yamamoto, K., Ichijo, H., and Korsmeyer, S. J. (1999) BCL-2 is phosphorylated and inactivated by an ASK1/Jun N-terminal protein kinase pathway normally activated at G(2)/M. *Mol. Cell. Biol.* **19,** 8469–8478 CrossRef Medline
42. Leung, K. T., Li, K. K., Sun, S. S., Chan, P. K., Ooi, V. E., and Chiu, L. C. (2008) Activation of the JNK pathway promotes phosphorylation and degradation of BimEL–a novel mechanism of chemoresistance in T-cell acute lymphoblastic leukemia. *Carcinogenesis* **29,** 544–551 Medline
43. Ley, R., Balmanno, K., Hadfield, K., Weston, C., and Cook, S. J. (2003) Activation of the ERK1/2 signaling pathway promotes phosphorylation and proteasome-dependent degradation of the BH3-only protein, Bim. *J. Biol. Chem.* **278,** 18811–18816 CrossRef Medline

44. Wajapeyee, N., Serra, R. W., Zhu, X., Mahalingam, M., and Green, M. R. (2008) Oncogenic BRAF induces senescence and apoptosis through pathways mediated by the secreted protein IGFBP7. *Cell* **132,** 363–374 CrossRef Medline
45. Choppara, S., Malonia, S. K., Sankaran, G., Green, M. R., and Santra, M. K. (2018) Degradation of FBXO31 by APC/C is regulated by AKT- and ATM-mediated phosphorylation. *Proc. Natl. Acad. Sci. U.S.A.* **115,** 998–1003 CrossRef Medline
46. Bradford, M. M. (1976) A rapid and sensitive method for the quantitation of microgram quantities of protein utilizing the principle of protein-dye binding. *Anal. Biochem.* **72,** 248–254 CrossRef Medline
47. Dimri, G. P., Lee, X., Basile, G., Acosta, M., Scott, G., Roskelley, C., Medrano, E. E., Linskens, M., Rubelj, I., and Pereira-Smith, O. (1995) A biomarker that identifies senescent human cells in culture and in aging skin *in vivo*. *Proc. Natl. Acad. Sci. U.S.A.* **92,** 9363–9367 CrossRef Medline
48. Sali, A., and Blundell, T. L. (1993) Comparative protein modelling by satisfaction of spatial restraints. *J. Mol. Biol.* **234,** 779–815 CrossRef Medline
49. Laskowski, R. A., MacArthur, M. W., Moss, D. S., and Thornton, J. M. (1993) PROCHECK: a program to check the stereochemical quality of protein structures. *J. Appl. Crystallogr.* **26,** 283–291 CrossRef
50. Colovos, C., and Yeates, T. O. (1993) Verification of protein structures: patterns of nonbonded atomic interactions. *Protein Sci.* **2,** 1511–1519 CrossRef Medline
51. Lüthy, R., Bowie, J. U., and Eisenberg, D. (1992) Assessment of protein models with three-dimensional profiles. *Nature* **356,** 83–85 CrossRef Medline
52. Pontius, J., Richelle, J., and Wodak, S. J. (1996) Deviations from standard atomic volumes as a quality measure for protein crystal structures. *J. Mol. Biol.* **264,** 121–136 CrossRef Medline
53. Wiederstein, M., and Sippl, M. J. (2007) ProSA-web: interactive web service for the recognition of errors in three-dimensional structures of proteins. *Nucleic Acids Res.* **35,** W407–W410 CrossRef Medline
54. Kaur, H., Garg, A., and Raghava, G. P. (2007) PEPstr: a *de novo* method for tertiary structure prediction of small bioactive peptides. *Protein Pept. Lett.* **14,** 626–631 CrossRef Medline
55. Morris, G. M., Huey, R., Lindstrom, W., Sanner, M. F., Belew, R. K., Goodsell, D. S., and Olson, A. J. (2009) AutoDock4 and AutoDockTools4: automated docking with selective receptor flexibility. *J. Comput. Chem.* **16,** 2785–2791 CrossRef Medline
56. Trott, O., and Olson, A. J. (2010) AutoDock Vina: improving the speed and accuracy of docking with a new scoring function, efficient optimization, and multithreading. *J. Comput. Chem.* **31,** 455–461 Medline